Journal of Science and Technology in Civil Engineering, HUCE (NUCE), 2022, 16 (3): 71–83

TOPOLOGY AND SIZE OPTIMIZATION FOR X-BRACING SYSTEM OF NONLINEAR INELASTIC SPACE STEEL FRAMES

Qui X. Lieu[a,b,*], Khanh D. Dang[a,b], Van Hai Luong[a,b], Son Thai[a,b]

[a]*Faculty of Civil Engineering, Ho Chi Minh City University of Technology (HCMUT), 268 Ly Thuong Kiet Street, District 10, Ho Chi Minh City, Vietnam*
[b]*Vietnam National University Ho Chi Minh City, Linh Trung Ward, Thu Duc City, Ho Chi Minh City, Vietnam*

Article history:
Received 06/5/2022, Revised 30/5/2022, Accepted 01/6/2022

Abstract

In this article, a Python-programmed advanced design paradigm is firstly introduced to topology and size optimization of the X-bracing system of nonlinear inelastic space steel frames. For that purpose, an advanced analysis method considering both geometric and material nonlinearities is utilized as an effective finite element analysis (FEA) solver. In which, X-bracing members are modeled by truss elements, while the beam and column members are simulated by beam-column ones. The bracing members' cross-sectional area and their position are respectively treated as discrete size and topology design variables. The problem aims to minimize the weight of X-bracing system so that the constraints on the strength, inter-story drift and maximum displacement are satisfied. An adaptive hybrid evolutionary firefly algorithm (AHEFA) is employed as an optimizer. Numerical examples are exhibited to illustrate the powerful ability of the present methodology.

Keywords: advanced design method; topology and size optimization; X-bracing system; nonlinear inelastic space steel frames; adaptive hybrid evolutionary firefly algorithm (AHEFA).

https://doi.org/10.31814/stce.huce(nuce)2022-16(3)-06

1. Introduction

For most steel structures, their bracing system often plays a crucial role in design to resist the impact of lateral loadings. Its core features include the position, cross-sectional area and the shape of bracing systems such as X-, K- and V-types. Nonetheless, these issues are often designed based on the guidelines and specifications of a specific standard as well as the practical experience of structural engineers. Such manners may not, therefore, result in the best outcomes. To tackle this knot, structural optimization has emerged as an effective design technique. In general, this field can be categorized into topology, size and shape optimization. All of them are the best tools that can deal well with all the foregoing requirements of designing bracing systems. Additionally, selecting a proper optimizer to find out high-quality optimal solutions to such problems is also a core issue.

With this regard, Gholizadeh and Poorhoseini [1] used an improved dolphin echolocation (IDE) algorithm to optimize the topology and size for the X-bracing system of planar steel frames under seismic loadings. Then, Gholizadeh and Ebadijalal [2] also optimize the X-bracing system's layout in 2D

*Corresponding author. *E-mail address:* lieuxuanqui@hcmut.edu.vn (Lieu, Q. X.)

steel frames subjected to seismic loadings by utilizing the center of mass optimization (CMO). In both works, the nonlinear behavior of bracings including plasticity and large deflection was implemented by OpenSees [3]. This platform takes account of the *P*-Δ effect by the corotational transformation technique, but the *P*-*δ* effect caused by the interaction between the axial force and bending moments is ignored. Consequently, the strength of a member under significant axial forces can not be estimated accurately. Moreover, the element nonlinear stiffness matrix is established based upon Hermite and linear interpolation functions for transverse and axial displacements. Therefore, that method requires many elements per member to achieve good accuracy. This leads to a time-consuming performance for the FEA process, especially for real large-scale structures.

To reduce the computational cost caused by the above issue, an advanced analysis method was suggested in the materials [4, 5]. In this approach, the stability functions which are obtained from the closed-form solution to a beam-column element under axial force and bending moments are employed to exactly represent its transverse displacement field. Thus, its *P*-*δ* and *P*-Δ phenomena can be precisely evaluated with only one or two elements per member. The material nonlinearity is treated by the refined plastic hinge framework. This strategy allows the plastic hinge formulation to only occur at two ends of an element via the Orbison surface [6] with a very simple implementation. Moreover, checking the separate strength for each of all members according to specification equations as that done in the works [1, 2] is not demanded since this method has the possibility of directly estimating the stability and ultimate strength of a structure and its every individual. A more comprehensive review of this paradigm was reported by Kim and Chen [7]. Owing to those advantages, this analysis approach was employed as an effective FEA solver in the size optimization process of nonlinear inelastic steel frames [8–10].

Nonetheless, there have been no reports regarding topology and size optimization for X-bracing systems of such structures under static loadings using the advanced analysis method associated with an effective metaheuristic algorithm until now. Accordingly, this work aims to suggest an advanced design method to achieve the above purpose as the first contribution. In which, X-bracing members are simulated by truss elements, while the beam and column members are modeled by beam-column ones. The bracing members' cross-sectional area and their position are respectively taken as discrete size and topology design variables. The constraints on the strength, inter-story drift and displacements are imposed to minimize the weight of the whole X-bracing system. The authors' previously developed AHEFA [11] is used as an optimizer. This algorithm has been also successfully applied for simultaneous topology, size and shape of trusses under the multiple restrictions of kinematic stability, stress, displacement, natural frequency and Euler buckling loading [12]. As an extension of the authors' work, the topology framework proposed in that study is adopted for the performance of this research. A computer code structure is programmed by Python 3.7 software on a laptop with Intel® CoreTM i7-2670QM CPU at 2.20GHz, 12.0GB RAM of memory, and Windows 7® Professional with 64-bit operating system.

2. Advanced analysis method

2.1. Beam-column element

a. Geometric nonlinear of *P*-*δ* effect

In this work, a beam-column element originally developed in the publications [4, 5] is adopted to take account of the second-order effect caused by the *P*-*δ* geometric nonlinear. This element utilizes the stability functions, which are attained from the closed-form solution to a beam-column member

under axial force and bending moment, to accurately describe its slope-deflection curve with only one or two elements per member. This method can dramatically save the computational cost against that of the traditional FEM due to using Hermite interpolation functions. Following this, the incremental force-displacement relationship can be expressed by

$$\begin{Bmatrix} P \\ M_{yA} \\ M_{yB} \\ M_{zA} \\ M_{zB} \\ T \end{Bmatrix} = \begin{bmatrix} \frac{EA}{L} & 0 & 0 & 0 & 0 & 0 \\ 0 & S_{1y}\frac{EI_y}{L} & S_{2y}\frac{EI_y}{L} & 0 & 0 & 0 \\ 0 & S_{2y}\frac{EI_y}{L} & S_{1y}\frac{EI_y}{L} & 0 & 0 & 0 \\ 0 & 0 & 0 & S_{1z}\frac{EI_z}{L} & S_{2z}\frac{EI_z}{L} & 0 \\ 0 & 0 & 0 & S_{2z}\frac{EI_z}{L} & S_{1z}\frac{EI_z}{L} & 0 \\ 0 & 0 & 0 & 0 & 0 & \frac{GJ}{L} \end{bmatrix} \begin{Bmatrix} \delta \\ \theta_{yA} \\ \theta_{yB} \\ \theta_{zA} \\ \theta_{zB} \\ \phi \end{Bmatrix} \tag{1}$$

where P, M_{yA}, M_{yB}, M_{zA}, M_{zB} and T denote the incremental axial force, end moments concerning y and z axes, and torsion, respectively; $\delta, \theta_{yA}, \theta_{yB}, \theta_{zA}, \theta_{zB}$ and ϕ stand for the incremental axial displacement, bending angles to y and z axes, and twist angle, respectively; E and G are the elastic and shear modulus. S_{1n} and S_{2n} $(n = y, z)$ are the stability functions corresponding to y and z axes, and given by

$$S_{1n} = \begin{cases} \dfrac{\pi\sqrt{\rho_n}\sin\left(\pi\sqrt{\rho_n}\right) - \pi^2\rho_n\cos\left(\pi\sqrt{\rho_n}\right)}{2 - 2\cos\left(\pi\sqrt{\rho_n}\right) - \pi\sqrt{\rho_n}\sin\left(\pi\sqrt{\rho_n}\right)}, & P < 0, \\ \dfrac{\pi^2\rho_n\cosh\left(\pi\sqrt{\rho_n}\right) - \pi\sqrt{\rho_n}\sinh\left(\pi\sqrt{\rho_n}\right)}{2 - 2\cosh\left(\pi\sqrt{\rho_n}\right) + \pi\sqrt{\rho_n}\sinh\left(\pi\sqrt{\rho_n}\right)}, & P > 0, \end{cases} \tag{2}$$

$$S_{2n} = \begin{cases} \dfrac{\pi^2\rho_n - \pi\sqrt{\rho_n}\sin\left(\pi\sqrt{\rho_n}\right)}{2 - 2\cos\left(\pi\sqrt{\rho_n}\right) - \pi\sqrt{\rho_n}\sin\left(\pi\sqrt{\rho_n}\right)}, & P < 0, \\ \dfrac{\pi\sqrt{\rho_n}\sinh\left(\pi\sqrt{\rho_n}\right) - \pi^2\rho_n}{2 - 2\cosh\left(\pi\sqrt{\rho_n}\right) + \pi\sqrt{\rho_n}\sinh\left(\pi\sqrt{\rho_n}\right)}, & P > 0, \end{cases} \tag{3}$$

where $\rho_n = \dfrac{P}{(\pi^2 EI_n/L^2)}; n = y, z$. To avoid the singularity of using Eqs. (2) and (3) in the range of $-2 \le \rho_n \le 2\,(n = y, z)$, the above two functions are rewritten as follows

$$S_{1n} = 4 + \frac{2\pi^2\rho_n}{15} - \frac{(0.01\rho_n + 0.543)\,\rho_n^2}{4 + \rho_n} - \frac{(0.004\rho_n + 0.285)\,\rho_n^2}{8.183 + \rho_n} \tag{4}$$

$$S_{2n} = 2 - \frac{\pi^2\rho_n}{30} + \frac{(0.01\rho_n + 0.543)\,\rho_n^2}{4 + \rho_n} - \frac{(0.004\rho_n + 0.285)\,\rho_n^2}{8.183 + \rho_n} \tag{5}$$

b. Material nonlinear

The gradual yielding along the member length under axial loads caused by residual stresses is considered by Column Research Council (CRC) tangent modulus concept. According to this, Chen

and Lui [4] suggested the CRC E_t as follows

$$\begin{cases} E_t = 1.0E, & P \le 0.5P_y \\ E_t = 4\dfrac{P}{P_y}\left(1 - \dfrac{P}{P_y}\right)E, & P > 0.5P_y \end{cases} \tag{6}$$

Nonetheless, the above equation can not represent well the gradual yielding of beam-columns elements simultaneously imposed by both larger bending moments and small axial forces. To tackle this shortcoming, a parabolic function based on the refined plastic hinge method is used to simulate the gradual stiffness degradation from the elastic stage to the step of a fully established plastic hinge at both ends of an element. Then, the incremental force-displacement relationship is now expressed as follows

$$\begin{Bmatrix} P \\ M_{yA} \\ M_{yB} \\ M_{zA} \\ M_{zB} \\ T \end{Bmatrix} = \begin{bmatrix} \dfrac{E_tA}{L} & 0 & 0 & 0 & 0 & 0 \\ 0 & k_{iiy} & k_{ijy} & 0 & 0 & 0 \\ 0 & k_{ijy} & k_{jjy} & 0 & 0 & 0 \\ 0 & 0 & 0 & k_{iiz} & k_{ijz} & 0 \\ 0 & 0 & 0 & k_{ijz} & k_{jjz} & 0 \\ 0 & 0 & 0 & 0 & 0 & \dfrac{GJ}{L} \end{bmatrix} \begin{Bmatrix} \delta \\ \theta_{yA} \\ \theta_{yB} \\ \theta_{zA} \\ \theta_{zB} \\ \phi \end{Bmatrix} \tag{7}$$

where

$$\begin{aligned} k_{iiy} &= \eta_A\left(S_1 - \frac{S_2^2}{S_1}(1-\eta_B)\right)\frac{E_tI_y}{L}, \quad k_{ijy} = \eta_A\eta_B S_2\frac{E_tI_y}{L}, \quad k_{jjy} = \eta_B\left(S_1 - \frac{S_2^2}{S_1}(1-\eta_A)\right)\frac{E_tI_y}{L}, \\ k_{iiz} &= \eta_A\left(S_3 - \frac{S_4^2}{S_3}(1-\eta_B)\right)\frac{E_tI_z}{L}, \quad k_{ijz} = \eta_A\eta_B S_4\frac{E_tI_z}{L}, \quad k_{jjz} = \eta_B\left(S_3 - \frac{S_4^2}{S_3}(1-\eta_A)\right)\frac{E_tI_z}{L} \end{aligned} \tag{8}$$

in which

$$\eta = \begin{cases} 1, & \alpha \le 0.5 \\ 4\alpha(1-\alpha), & 0.5 < \alpha \le 1.0 \\ 0, & \alpha > 1.0 \end{cases} \tag{9}$$

and the Orbison yield surface α [6] is defined as follows

$$\alpha = 1.15p^2 + m_z^2 + m_y^4 + 3.67p^2m_z^2 + 3.0p^6m_y^2 + 4.65m_z^4m_y^2 - 1 \tag{10}$$

where $p = P/P_y$; $m_y = M_y/M_{py}$ (weak axis); $m_z = M_z/M_{pz}$ (strong axis). P_y, M_{py} and M_{pz} denote the squash load and plastic moment capacity with regard to y and z axes, respectively.

c. Shear deformation effect

To take account of the shear deformation effect on the beam-column element's nonlinear behavior, the incremental force-displacement relationship defined in Eq. (7) is modified as follows

$$\begin{Bmatrix} P \\ M_{yA} \\ M_{yB} \\ M_{zA} \\ M_{zB} \\ T \end{Bmatrix} = \begin{bmatrix} \dfrac{E_tA}{L} & 0 & 0 & 0 & 0 & 0 \\ 0 & C_{iiy} & C_{ijy} & 0 & 0 & 0 \\ 0 & C_{ijy} & C_{jjy} & 0 & 0 & 0 \\ 0 & 0 & 0 & C_{iiz} & C_{ijz} & 0 \\ 0 & 0 & 0 & C_{ijz} & C_{jjz} & 0 \\ 0 & 0 & 0 & 0 & 0 & \dfrac{GJ}{L} \end{bmatrix} \begin{Bmatrix} \delta \\ \theta_{yA} \\ \theta_{yB} \\ \theta_{zA} \\ \theta_{zB} \\ \phi \end{Bmatrix} = \mathbf{K}_0^e \begin{Bmatrix} \delta \\ \theta_{yA} \\ \theta_{yB} \\ \theta_{zA} \\ \theta_{zB} \\ \phi \end{Bmatrix} \tag{11}$$

where

$$C_{iiy} = \frac{k_{ii}k_{jj} - k_{ij}^2 + k_{ii}A_{sz}GL}{k_{ii} + k_{jj} + 2k_{ij} + A_{sz}GL}, \quad C_{ijy} = \frac{-k_{ii}k_{jj} + k_{ij}^2 + k_{ij}A_{sz}GL}{k_{ii} + k_{jj} + 2k_{ij} + A_{sz}GL}$$
$$C_{jjy} = \frac{k_{ii}k_{jj} - k_{ij}^2 + k_{jj}A_{sz}GL}{k_{ii} + k_{jj} + 2k_{ij} + A_{sz}GL}, \quad C_{iiz} = \frac{k_{ii}k_{jj} - k_{ij}^2 + k_{ii}A_{sy}GL}{k_{ii} + k_{jj} + 2k_{ij} + A_{sy}GL} \tag{12}$$
$$C_{ijz} = \frac{-k_{ii}k_{jj} + k_{ij}^2 + k_{ij}A_{sy}GL}{k_{ii} + k_{jj} + 2k_{ij} + A_{sy}GL}, \quad C_{jjz} = \frac{k_{ii}k_{jj} - k_{ij}^2 + k_{jj}A_{sy}GL}{k_{ii} + k_{jj} + 2k_{ij} + A_{sy}GL}$$

in which A_{sy} and A_{sz} stand for the shear areas of y and z axes, respectively. And $A_{sy} = A_{sz} = A/1.2$ for rectangular sections.

d. Element stiffness matrix

The element stiffness matrix without side sway is given in its local system as follows

$$\mathbf{K}_{ns}^e = \mathbf{R}^T \mathbf{K}_0^e \mathbf{R} \tag{13}$$

where

$$\mathbf{R} = \begin{bmatrix} -1 & 0 & 0 & 0 & 0 & 0 & 1 & 0 & 0 & 0 & 0 & 0 \\ 0 & 0 & -\frac{1}{L} & 0 & 1 & 0 & 0 & 0 & \frac{1}{L} & 0 & 0 & 0 \\ 0 & 0 & -\frac{1}{L} & 0 & 0 & 0 & 0 & 0 & \frac{1}{L} & 0 & 1 & 0 \\ 0 & \frac{1}{L} & 0 & 0 & 0 & 1 & 0 & -\frac{1}{L} & 0 & 0 & 0 & 0 \\ 0 & \frac{1}{L} & 0 & 0 & 0 & 0 & 0 & -\frac{1}{L} & 0 & 0 & 0 & 1 \\ 0 & 0 & 0 & 1 & 0 & 0 & 0 & 0 & 0 & -1 & 0 & 0 \end{bmatrix} \tag{14}$$

and $\mathbf{K}_0^e$ is derived from Eq. (11).

Now, the local element stiffness matrix with its sway (P-Δ effect) is computed by

$$\mathbf{K}_s = \begin{bmatrix} \mathbf{G}_s & -\mathbf{G}_s \\ -\mathbf{G}_s{}^T & \mathbf{G}_s \end{bmatrix} \tag{15}$$

where

$$\mathbf{G}_s = \begin{bmatrix} 0 & (M_{zA} + M_{zB})/L^2 & -\left(M_{yA} + M_{yB}\right)/L^2 & 0 & 0 & 0 \\ (M_{zA} + M_{zB})/L^2 & P/L & 0 & 0 & 0 & 0 \\ -\left(M_{yA} + M_{yB}\right)/L^2 & 0 & P/L & 0 & 0 & 0 \\ 0 & 0 & 0 & 0 & 0 & 0 \\ 0 & 0 & 0 & 0 & 0 & 0 \\ 0 & 0 & 0 & 0 & 0 & 0 \end{bmatrix} \tag{16}$$

Finally, the local element stiffness matrix considering both geometric (P-δ and P-Δ) and material nonlinearities is given as

$$\mathbf{K}^e = \mathbf{K}_{ns}^e + \mathbf{K}_s^e \tag{17}$$

Note that a matrix $\mathbf{T}$ [13] is required to transform from the local stiffness matrix and inner-force vector of a beam-column element to the corresponding global ones and vice versa.

2.2. *Truss element*

a. Geometric nonlinear

Herein, the geometric nonlinear effect of a truss member is constructed based on the updated Lagrangian formulation. According to Yang and Kuo [13], the nonlinear equilibrium equation of a typical truss element is expressed as follows

$$\left(\mathbf{k}_E^e + \mathbf{k}_G^e + \mathbf{s}_1^e + \mathbf{s}_2^e + \mathbf{s}_3^e\right)\mathbf{u}_e + {}^1f^e = {}^2f^e \tag{18}$$

where ${}^1f^e$ is the local initial nodal forces of the eth element at the last known configuration C_1, while ${}^2f^e$ is the local total nodal forces of the eth element at the current configuration C_2. $\mathbf{k}_E^e$ and $\mathbf{k}_G^e$ are the local elastic and geometric stiffness matrices of the eth element, and are respectively given as follows

$$\mathbf{k}_E^e = \frac{EA}{L}\begin{bmatrix} 1 & 0 & 0 & -1 & 0 & 0 \\ 0 & 0 & 0 & 0 & 0 & 0 \\ 0 & 0 & 0 & 0 & 0 & 0 \\ -1 & 0 & 0 & 1 & 0 & 0 \\ 0 & 0 & 0 & 0 & 0 & 0 \\ 0 & 0 & 0 & 0 & 0 & 0 \end{bmatrix}, \quad \mathbf{k}_G^e = \frac{P}{L}\begin{bmatrix} 1 & 0 & 0 & -1 & 0 & 0 \\ 0 & 1 & 0 & 0 & -1 & 0 \\ 0 & 0 & 1 & 0 & 0 & -1 \\ -1 & 0 & 0 & 1 & 0 & 0 \\ 0 & -1 & 0 & 0 & 1 & 0 \\ 0 & 0 & -1 & 0 & 0 & 1 \end{bmatrix}. \tag{19}$$

The higher-order stiffness terms of $\mathbf{s}_1^e, \mathbf{s}_2^e$ and $\mathbf{s}_3^e$ are respectively provided below

$$\mathbf{s}_1^e = \frac{EA}{2L^2}\begin{bmatrix} \Delta u & \Delta v & \Delta w & -\Delta u & -\Delta v & -\Delta w \\ 0 & 0 & 0 & 0 & 0 & 0 \\ 0 & 0 & 0 & 0 & 0 & 0 \\ -\Delta u & -\Delta v & -\Delta w & \Delta u & \Delta v & \Delta w \\ 0 & 0 & 0 & 0 & 0 & 0 \\ 0 & 0 & 0 & 0 & 0 & 0 \end{bmatrix} \tag{20}$$

$$\mathbf{s}_2^e = \frac{EA}{2L^2}\begin{bmatrix} 2\Delta u & 0 & 0 & -2\Delta u & 0 & 0 \\ \Delta v & \Delta u & 0 & -\Delta v & -\Delta u & 0 \\ \Delta w & 0 & \Delta u & -\Delta w & 0 & \Delta u \\ -2\Delta u & 0 & 0 & 2\Delta u & 0 & 0 \\ -\Delta v & -\Delta u & 0 & \Delta v & \Delta u & 0 \\ -\Delta w & 0 & -\Delta u & \Delta w & 0 & \Delta u \end{bmatrix} \tag{21}$$

$$\mathbf{s}_3^e = \frac{EA}{6L^3}\begin{bmatrix} \mathbf{\Lambda} & -\mathbf{\Lambda} \\ -\mathbf{\Lambda} & \mathbf{\Lambda} \end{bmatrix} \tag{22}$$

with

$$\mathbf{\Lambda} = \begin{bmatrix} 3\Delta u^2 + \Delta v^2 + \Delta w^2 & 2\Delta u\Delta v & 2\Delta u\Delta w \\ 2\Delta u\Delta v & \Delta u^2 + 3\Delta v^2 + \Delta w^2 & 2\Delta v\Delta w \\ 2\Delta u\Delta w & 2\Delta v\Delta w & \Delta u^2 + \Delta v^2 + 3\Delta w^2 \end{bmatrix} \tag{23}$$

and

$$\Delta u = u_{x,2}^e - u_{x,1}^e; \Delta v = u_{y,2}^e - u_{y,1}^e; \Delta w = u_{z,2}^e - u_{z,1}^e \tag{24}$$

Note that the same transform matrix $\mathbf{T}$ of beam-column elements [13] is utilized to switch from the local stiffness matrix and inner-force vector of a truss element to the corresponding global ones and vice versa.

b. Material nonlinear

According to Hill et al. [14], the stress-strain relationship to describe the material nonlinear, i.e. inelastic post-buckling behavior, of compressive truss members is given by

$$\begin{aligned} &\sigma = E\varepsilon, && |\varepsilon| \le \varepsilon_{cr} \\ &\sigma = \sigma_{cr}, && \varepsilon_{cr} \le |\varepsilon| \le \varepsilon_0 \\ &\sigma(\varepsilon) = \sigma_l + (\sigma_{cr} - \sigma_l)\, e^{-\left(X_1 + X_2\sqrt{\varepsilon'}\right)\varepsilon'}, && |\varepsilon| > \varepsilon_0 \end{aligned} \tag{25}$$

where $\sigma_l = 0.4\sigma_{cr}$ is the asymptotic lower stress limit; X_1 and X_2 are the constants depending on the slenderness ratio, and are taken to be 50 and 100, respectively; ε' is the axial strain measured from the start of inelastic post-buckling response; $\varepsilon = \varepsilon_L + \varepsilon_{NL}$ is the updated Green strain increment with

$$\varepsilon_L = \frac{du}{dx} = \frac{\Delta u}{L_0}, \quad \text{and} \quad \varepsilon_{NL} = \frac{1}{2}\left[\left(\frac{du}{dx}\right)^2 + \left(\frac{dv}{dx}\right)^2 + \left(\frac{dw}{dx}\right)^2\right] = \frac{1}{2}\left[\left(\frac{\Delta u}{dx}\right)^2 + \left(\frac{\Delta v}{dx}\right)^2 + \left(\frac{\Delta w}{dx}\right)^2\right] \tag{26}$$

Assume that the yield strain is neglected, then $\varepsilon_0 = \varepsilon_{cr} = \varepsilon'$. The Euler critical buckling stress σ_{cr} and the corresponding strain ε_{cr} are respectively given as

$$\sigma_{cr} = \frac{\pi^2 EI}{AL_0^2} \quad \text{and} \quad \varepsilon_{cr} = \frac{\sigma_{cr}}{E} \tag{27}$$

where E is the elastic Young's modulus; I, A and L_0 are the inertia moment of weak axis, cross-sectional area and length of truss element, respectively.

To consider the inelastic effect as $|\varepsilon| > \varepsilon_0$, the tangent modulus E_T is given as

$$E_T = \left(\frac{d\sigma}{d\varepsilon}\right)\left(\frac{L_1}{L_0}\right)^3 \tag{28}$$

where the term $\left(\frac{L_1}{L_0}\right)^3$ is for the large strain transformation; L_0 and L_1 are the undeformed and deformed length of the truss member, respectively.

2.3. Geometric imperfections

Geometric imperfections often caused by the tolerance of fabrication and erection can be modeled by the following three ways: (i) explicit imperfection; (ii) equivalent notional load, and (iii) reduced tangent modulus. For space structures, reducing the tangent modulus is the simplest and most effective manner compared with the others, yet still providing accurate solutions with high reliability. Therefore, $E_T' = 0.85E_T$ is adopted in this work. Note that modeling geometric imperfections are only for beam-column elements, but not for truss ones of the X-bracing system [7].

3. Optimization problem

3.1. Problem statement

The problem aims to determine the best position and optimal cross-sectional area of X-bracing members of inelastic space steel frames considering geometric behavior. This objective function is to minimize the weight of the whole X-bracing system so that the constraints on the strength, inter-story

drift and displacement are satisfied. The truss element is dedicated to modeling X-bracing members, while the beam-column element is devoted to simulating the beam and column ones. Their cross-sectional area is treated as a discrete design variable, while their optimal position is taken as a discrete topology one. A mathematical statement of this problem is given as follows

$$\begin{aligned} &\text{Minimize:} \quad W(\mathbf{X}) = \sum_{i=1}^{nb} \rho_i A_i L_i, \\ &\text{Subjected to:} \quad \begin{cases} \mathbf{KU} = \mathbf{F}, \\ C_1 = 1 - LF \le 0, \\ C_2 = \dfrac{|d_s|}{[d_s]} - 1 \le 0, \quad s = 1, 2, ..., n_{story}, \\ C_3 = \dfrac{|u_j|}{\left[u_j\right]} - 1 \le 0, \quad j = 1, 2, ..., n_{dof}, \\ A_i^{\min} \le A_i \le A_i^{\max}, \end{cases} \end{aligned} \tag{29}$$

where $W(\mathbf{X})$ is the weight of the whole X-bracing system; ρ_i, A_i and L_i denote the density, cross-sectional area and length of the ith bracing member, respectively; nb stands for the whole number of bracing members; And $\mathbf{X}$ is the design variable vector including size one $\mathbf{A} = \{A_1, ..., A_i, ..., A_{nb}\}$ and topology pseudo-are one $\mathbf{I} = \{I_1, ..., I_i, ..., I_{nb}\}$, in which $I_i = 1$ denotes the bracing member's attendance, while $I_i = 0$ symbolizes for the removed bracing member; $\mathbf{K}$, $\mathbf{U}$ and $\mathbf{F}$ are the global stiffness matrix, the global DOF vector and the global applied load vector, respectively. The constraint C_1 is dedicated to checking the load-carrying capacity of the structural system; $LF = R/Q$ is the load factor, where R is the load-carrying capacity, and Q is the load effect. The constraint C_2 is devoted to testing the inter-story drift, where d_s and $[d_s]$ are the sth inter-story drift and its corresponding allowable limitation, respectively. The constraint C_3 is used for restricting the horizontal displacement, where u_j and $\left[u_j\right]$ are the horizontal displacement of the ith DOF and its corresponding allowable limitation, respectively. $A_i^{\min}$ and $A_i^{\max}$ are the upper and lower boundaries of A_i, respectively.

The constrained optimization problem defined in Eq. (29) is transformed into a corresponding unconstrained one by the penalty function strategy. Its expression is now given as

$$W_{\text{penalty}}(\mathbf{X}) = \sum_{i=1}^{nb} \rho_i A_i L_i + \lambda \left[\sum_{r}^{ns} \max(0, C_r)\right]^2 \tag{30}$$

where λ is the penalty parameter which is chosen to be 10^5 in this work. r is the rth constraint, and ns is the whole number of restrictions.

3.2. Optimizer

In this work, the AHEFA which was previously developed in the authors' publication [11] is utilized as an optimizer to find the optimal solution to the above-stated problem. This algorithm has proven its reliability and efficiency against numerous metaheuristic approaches in the above-cited material. Moreover, it has been also successfully applied for optimization of functionally graded (FG) plates [15–17], reliability-based design optimization (RBDO) of FG plates [18], structural healthy monitoring (SHM) [19], and even simultaneous topology, size and shape of trusses [12]. Interesting readers are suggested to consult the reference [11] for more detailed information.

4. Numerical examples

4.1. Verification

Fig. 1 shows a two-story space steel space under static loadings and its problem parameters. This example was previously investigated by De Souza [20] employing the force-based method with the fiber hinge method, and solved by the arc-length procedure. Abbasnia and Kassimali [21] used the large deformation elastic-plastic method based on the beam-column theory and the ideally elastic-plastic hinge, and resolved by the Newton–Raphson algorithm. Thai and Kim [22] used the Fortran-programmed advanced analysis approach based on the stability function and the refined plastic hinge method to examine this example. In that work, the generalized displacement control (GDC) approach was used. Then, Thai and Kim [23] also employed the fiber method to capture the inelastic effect. In this study, the Newton–Raphson algorithm [24] is utilized to solve the above nonlinear equation system.

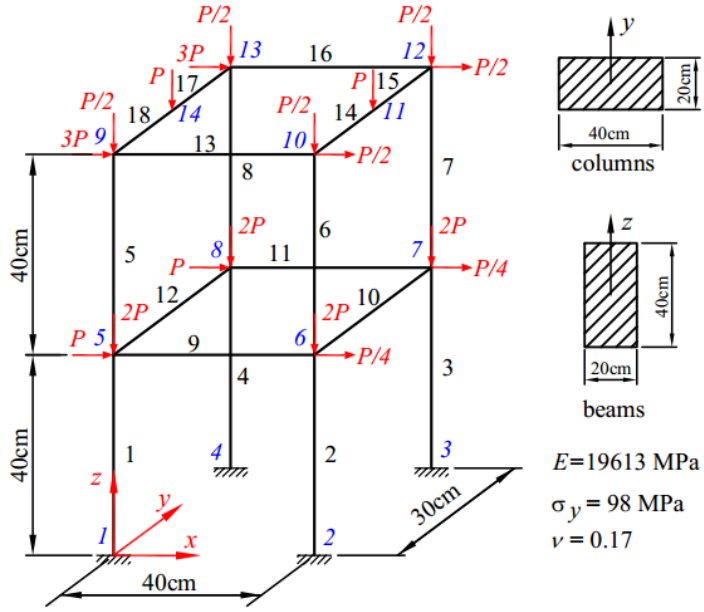

Figure 1. A two-story space steel frame

The ultimate load obtained by different researches is reported in Table 1. It can be found that the ultimate load provided by the present study is of a good agreement with that of other publications, namely its error against [20] is 0.59% which is better than 0.78% of Ref. [21], and 0.6% of Ref. [23], but is slightly higher than 0.35% of Ref. [22]. The reason is more powerful iterative-incremental algorithms were used in Refs. [20, 22] to trace the nonlinear curve. Nonetheless, the Newton-Raphson method is a simpler and more appropriate solver when combined with optimization problems. Moreover, the relationship between the load factor and the x-axis displacement at node 13 is shown in Fig. 2. As observed, the curve obtained by the present work matches well with that of other studies. This has confirmed the reliability and accuracy of Python code structure programmed by the authors. Therefore, it is used as an effective FEA solver to optimize topology and size for the X-bracing system of nonlinear inelastic space steel frames in the next example.

Table 1. Comparison of the ultimate load obtained by different researches

Research	Ultimate load, kN	Error, %
De Souza [20]	128.05	-
Abbasnia and Kassimali [21]	129.05	0.78
Thai and Kim [22]	128.50	0.35
Thai and Kim [23]	128.82	0.60
This study	127.30	0.59

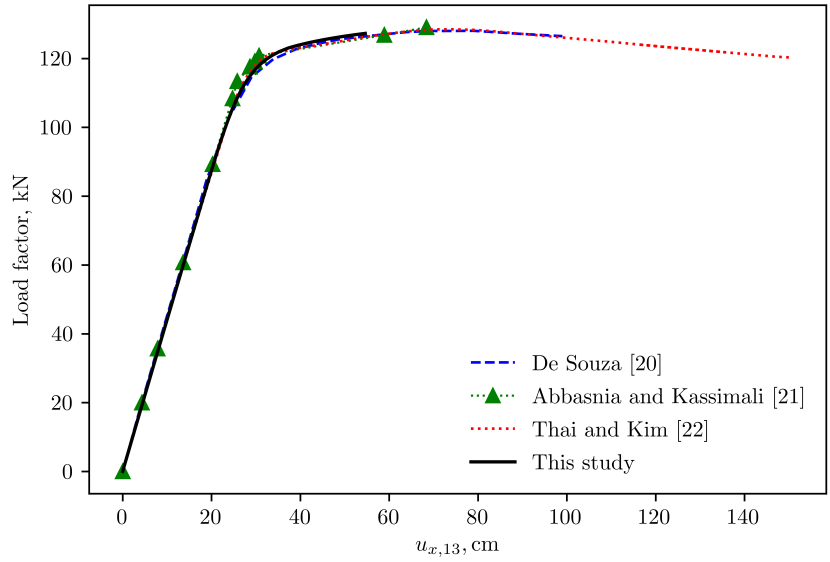

Figure 2. The load factor and the x-axis displacement at node 13

4.2. Present study

To illustrate the capability of the proposed paradigm in optimizing the topology and size of truss members in the X-bracing system of nonlinear inelastic space steel frames, a ground structure as shown in Fig. 3 is examined. This braced structure is modified from the two-story frame of the previous example. In this example, there are 16 size and 16 topology variables in total. The cross-sectional area of bracing members is discretely assigned according to a discrete dataset [12] given by the American Institute of Steel Construction (AISC). Note that the same mean diameter-wall thickness ratio of 10.0 is assumed for all tubular sections. The buckling coefficient of $k = 4.0$ is therefore employed to compute the Euler buckling condition of all members with the inertia moment of weak axis being $I = 4A^2/\pi^2$. The material density is assumed to be 7850 kg/m^3. The allowable inter-story drift is $h/500$, where $h = 4$ m is the story height. In addition, the maximum displacement is limited by $H/400$, where $H = 8$ m is the structural height. Assume that all members'cross sections are compact, and thus there are no local buckling and lateral-torsional buckling phenomena. The population size is chosen to be 20, 10 independent runs are performed for each of all investigated cases. Statistical results including the best weight and the corresponding number of objective function evaluations (No. OFEs), the worst weight, mean weight, standard deviation (SD) and feasible topologies are reported. Other parameters and the stopping criteria are set up as those provided by Lieu [12].

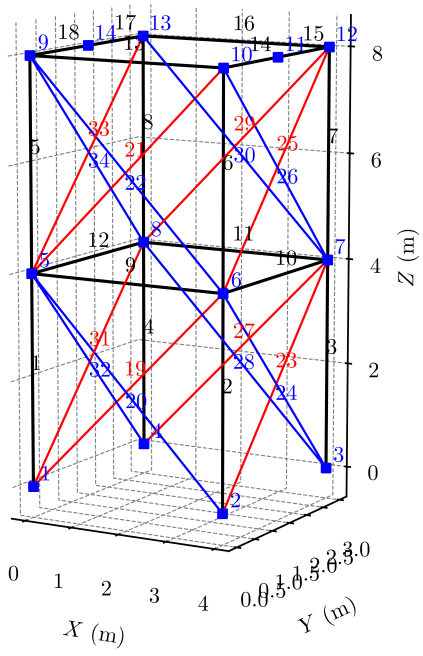

Figure 3. A ground structure of a braced two-story space steel frame

Table 2. Optimal results obtained for two cases

A_i (cm^2)	Case 1	Case 2
A_{19}	16.9032	28.9677
A_{20}	-	180.6448
A_{21}	16.9032	89.6772
A_{22}	-	89.6772
A_{27}	16.9032	87.0966
A_{28}	-	121.2901
A_{29}	22.9032	69.9999
A_{30}	-	121.2901
Best weight (kg)	326.5203	3561.5780
No. OFEs	6120	8200
Worst weight (kg)	406.9106	3727.1635
Average weight (kg)	361.5838	3610.7828
SD	38.8323	64.6084
Feasible topologies	20	20
Load factor, LF	1.000	1.000
Max displacement (m)	0.0200	0.0200
Max inter-story drift	0.0026	0.025

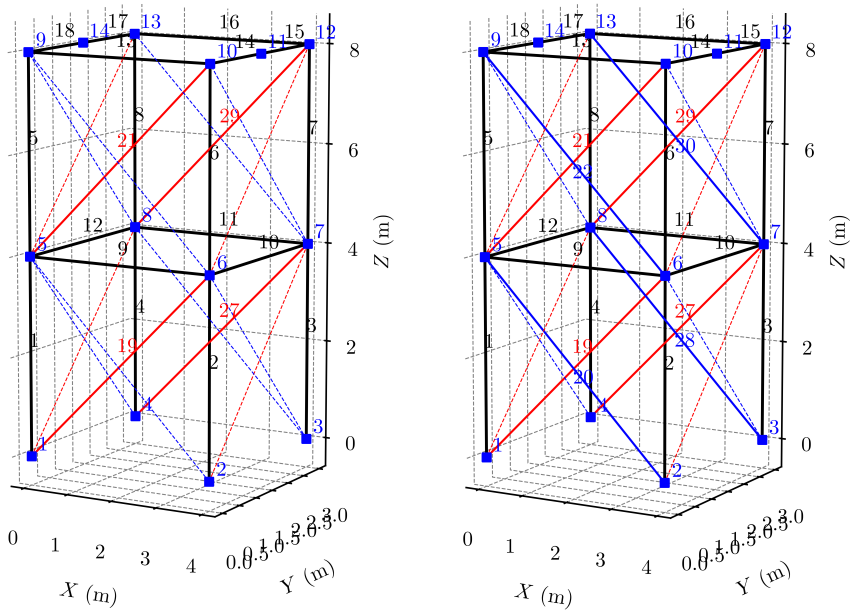

(a) Case 1 (b) Case 2

Figure 4. The topology results of X-bracing system for two cases

Optimal outcomes attained for two applied loading cases with $P = 10$ kN and $P = 50$ kN are summarized in Table 2. The topology results of X-bracing system are plotted in Fig. 4. The red and

blue dash lines symbolize the removed bracing members. It is obvious that when the applied loading increases, the X-bracing system requires more members to combat that load. Moreover, because loadings are only applied in the x and z axes, there are no bracing members in the y axis. The convergence history of weight and No. OFEs for both cases are given in Fig. 5.

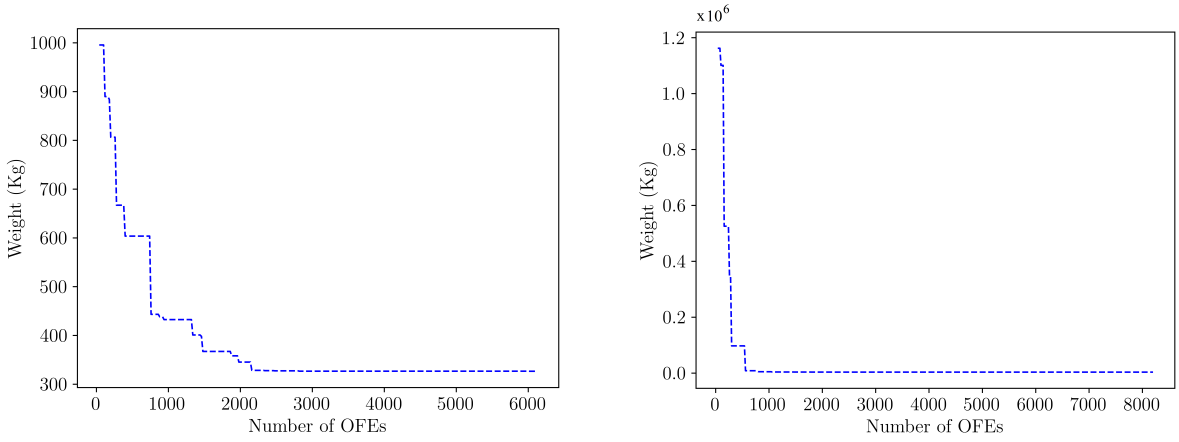

(a) Case 1 (b) Case 2

Figure 5. The weight convergence history for two cases

5. Conclusions

In this paper, the so-called advanced design method has been successfully developed for topology and size optimization of the X-bracing system of inelastic space steel frames with geometric nonlinear responses. The cross-sectional area of bracing members is treated as a discrete size design variable, whilst its position is taken as a discrete topology one. The objective function is to minimize the weight of the whole X-bracing system with the constraints on the strength, inter-story drift and displacements. To reduce the computational cost, an advanced analysis method is adopted as an FEA solver. In which, X-bracing members are simulated by truss elements, while the beam and column members are modeled by beam-column ones. The AHEFA is utilized as an optimization tool. The Python-coded computer program is built and verified for its reliability and accuracy through a two-story steel space frame. Outcomes obtained in the optimization example have indicated that the present methodology can reliably and efficiently determine the best position and optimal cross-sectional areas of the X-bracing system. Therefore, the suggested paradigm can be applied to topology, size and shape optimization for the bracing system of nonlinear inelastic space steel frames under seismic loadings, even strictly following load and resistance factor design (LRFD). And this topic will be carried out soon in near future.

Acknowledgements

This research is funded by Vietnam National University Ho Chi Minh City (VNU-HCM) under grant number C2021-20-33. We would like to thank Ho Chi Minh City University of Technology (HCMUT), VNU-HCM for the support of time and facilities for this study.

References

[1] Gholizadeh, S., Poorhoseini, H. (2016). Seismic layout optimization of steel braced frames by an improved dolphin echolocation algorithm. *Structural and Multidisciplinary Optimization*, 54(4):1011–1029.

[2] Gholizadeh, S., Ebadijalal, M. (2018). Performance based discrete topology optimization of steel braced frames by a new metaheuristic. *Advances in Engineering Software*, 123:77–92.

[3] McKenna, F. (2011). OpenSees: A framework for earthquake engineering simulation. *Computing in Science & Engineering*, 13(4):58–66.

[4] Chen, W.-K., Lui, E. M. (1987). *Structural stability: Theory and implementation*. PTR Prentice Hall.

[5] Chen, W. F., Sohal, I. (1995). *Plastic design and second-order analysis of steel frames*. Springer New York.

[6] Orbison, J. G., McGuire, W., Abel, J. F. (1982). Yield surface applications in nonlinear steel frame analysis. *Computer Methods in Applied Mechanics and Engineering*, 33(1-3):557–573.

[7] Chen, W. F., Lui, E. M. (2005). *Principles of structural design*. CRC Press.

[8] Truong, V. H., Kim, S.-E. (2017). An efficient method for reliability-based design optimization of nonlinear inelastic steel space frames. *Structural and Multidisciplinary Optimization*, 56(2):331–351.

[9] Truong, V.-H., Nguyen, P.-C., Kim, S.-E. (2017). An efficient method for optimizing space steel frames with semi-rigid joints using practical advanced analysis and the micro-genetic algorithm. *Journal of Constructional Steel Research*, 128:416–427.

[10] Truong, V.-H., Kim, S.-E. (2018). A robust method for optimization of semi-rigid steel frames subject to seismic loading. *Journal of Constructional Steel Research*, 145:184–195.

[11] Lieu, Q. X., Do, D. T. T., Lee, J. (2018). An adaptive hybrid evolutionary firefly algorithm for shape and size optimization of truss structures with frequency constraints. *Computers & Structures*, 195:99–112.

[12] Lieu, Q. X. (2022). A novel topology framework for simultaneous topology, size and shape optimization of trusses under static, free vibration and transient behavior. *Engineering with Computers*.

[13] Yang., Y.-B., Kuo, S.-R. (1994). *Theory & analysis of nonlinear framed structures*. Prentice Hall.

[14] Hill, C. D., Blandford, G. E., Wang, S. T. (1989). Post-buckling analysis of steel space trusses. *Journal of Structural Engineering*, 115(4):900–919.

[15] Lieu, Q. X., Lee, J. (2017). Modeling and optimization of functionally graded plates under thermo-mechanical load using isogeometric analysis and adaptive hybrid evolutionary firefly algorithm. *Composite Structures*, 179:89–106.

[16] Lieu, Q. X., Lee, J., Lee, D., Lee, S., Kim, D., Lee, J. (2018). Shape and size optimization of functionally graded sandwich plates using isogeometric analysis and adaptive hybrid evolutionary firefly algorithm. *Thin-Walled Structures*, 124:588–604.

[17] Lieu, Q. X., Lee, J. (2019). An isogeometric multimesh design approach for size and shape optimization of multidirectional functionally graded plates. *Computer Methods in Applied Mechanics and Engineering*, 343:407–437.

[18] Lieu, Q. X., Lee, J. (2019). A reliability-based optimization approach for material and thickness composition of multidirectional functionally graded plates. *Composites Part B: Engineering*, 164:599–611.

[19] Lieu, Q. X., Luong, V. H., Lee, J. (2019). Structural damage identification using adaptive hybrid evolutionary firefly algorithm. In *Springer Tracts in Nature-Inspired Computing*, Springer Singapore, 75–97.

[20] Souza, R. M. D. (2000). *Force-based finite element for large displacement inelastic analysis of frames*.

[21] Abbasnia, R., Kassimali, A. (1995). Large deformation elastic-plastic analysis of space frames. *Journal of Constructional Steel Research*, 35(3):275–290.

[22] Thai, H.-T., Kim, S.-E. (2009). Practical advanced analysis software for nonlinear inelastic analysis of space steel structures. *Advances in Engineering Software*, 40(9):786–797.

[23] Thai, H.-T., Kim, S.-E. (2011). Nonlinear inelastic analysis of space frames. *Journal of Constructional Steel Research*, 67(4):585–592.

[24] McGuire, W., Gallagher, R. H., Ziemian, R. D. (2015). *Matrix structural analysis*. Wiley.